AMERICAN SOCIETY FOR MICROBIOLOGY | Journal of Virology®

VACCINES AND ANTIVIRAL AGENTS

Mutations in Porcine Epidemic Diarrhea Virus nsp1 Cause Increased Viral Sensitivity to Host Interferon Responses and Attenuation *In Vivo*

Xiaoyu Niu,[a,b] Fanzhi Kong,[a,c] Jiayu Xu,[a,b] Mingde Liu,[a,b] Qiuhong Wang[a,b]

[a]Center for Food Animal Health, Department of Animal Sciences, College of Food, Agricultural and Environmental Sciences, The Ohio State University, Wooster, Ohio, USA

[b]Department of Veterinary Preventive Medicine, College of Veterinary Medicine, The Ohio State University, Columbus, Ohio, USA

[c]College of Animal Science and Veterinary Medicine, Heilongjiang Bayi Agricultural University, Daqing, Heilongjiang, China

ABSTRACT Coronavirus (CoV) nonstructural protein 1 (nsp1) inhibits cellular gene expression and antagonizes interferon (IFN) response. Porcine epidemic diarrhea virus (PEDV) infects pigs and causes high mortality in neonatal piglets. We hypothesized that a recombinant PEDV carrying mutations at the conserved residues N93 and N95 of nsp1 induces higher IFN responses and is more sensitive to IFN responses, leading to virus attenuation. We mutated PEDV nsp1 N93 and N95 to A93 and A95 to generate the recombinant N93/95A virus using the infectious clone of a highly virulent PEDV strain, PC22A (icPC22A), and evaluated N93/95A virus *in vitro* and *in vivo*. Compared with icPC22A, the N93/95A mutant replicated to significantly lower infectious titers, triggered stronger type I and III IFN responses, and was more sensitive to IFN treatment *in vitro*. To evaluate the pathogenicity and immunogenicity, 5-day-old gnotobiotic piglets were orally inoculated with the N93/95A or icPC22A strain or mock inoculated and then challenged at 22 days postinoculation (dpi) with icPC22A. icPC22A in all pigs (100% [5/5]) caused severe diarrhea and death within 6 dpi. Only one pig (25% [1/4]) died in the N93/95A group. Compared with the icPC22A group, significantly delayed and diminished fecal PEDV shedding was detected in the N93/95A group. Postchallenge, all piglets in N93/95A group were protected from severe diarrhea and death, whereas all pigs in the mock-challenged group developed severe diarrhea, and 25% (1/4) of them died. In summary, nsp1 N93A and N95A mutations attenuated PEDV but retained viral immunogenicity and can be targets for the development of live attenuated vaccines for PEDV.

IMPORTANCE PEDV causes porcine epidemic diarrhea (PED) and remains a great threat to the swine industry worldwide because no effective vaccines are available yet. Safe and effective live attenuated vaccines can be designed using reverse genetics to induce lactogenic immunity in pregnant sows to protect piglets from the deadly PED. We found that an engineered PEDV mutant carrying N93A and N95A mutations of nsp1 was partially attenuated and remained immunogenic in neonatal pigs. Our study suggested that nsp1 N93 and N95 can be good targets for the rational design of live attenuated vaccines for PEDV using reverse genetics. Because CoV nsp1 is conserved among alphacoronaviruses (α-CoVs) and betacoronaviruses (β-CoVs), it may be a good target for vaccine development for other α-CoVs or β-CoVs.

KEYWORDS nsp1, interferon, porcine epidemic diarrhea virus, porcine epidemic diarrhea, coronavirus, vaccine, veterinary vaccine development

Porcine epidemic diarrhea virus (PEDV) causes porcine epidemic diarrhea (PED), which is a highly contagious acute enteric disease characterized by watery diarrhea, vomiting, and severe dehydration in neonatal pigs. The disease was initially reported in England (1)

Editor Bryan R. G. Williams, Hudson Institute of Medical Research

Address correspondence to Qiuhong Wang, wang.655@osu.edu.

The authors declare no conflict of interest.

Received 17 March 2022
Accepted 19 April 2022
Published 18 May 2022

and Belgium (2) in the early 1970s. Recently, highly virulent strains emerged in China in 2010 and spread quickly to many other Asian countries (3–5). PEDV was introduced into the United States in 2013 and rapidly spread nationwide throughout the country (6). PEDV infection in suckling piglets can cause up to 100% mortality. It led to almost 10% loss of domestic pig population for the U.S. pig industry during the 2013-2014 outbreaks and posed a great threat to pork industry (7, 8).

PEDV is a member of *Alphacoronavirus* genus in the *Coronaviridae* family of the *Nidovirales* order. It is an enveloped virus possessing an approximately 28,000-nucleotide-long, positive-sense, single-stranded RNA genome with a 5′ cap and a 3′ polyadenylated tail (2). The PEDV genome contains two large open reading frames (ORFs), ORF1a and ORF1b, at the 5′ two-thirds of the genome, followed by the ORFs for four structural proteins and one accessory protein: the spike (S), ORF3, envelope (E), membrane (M), and nucleocapsid (N) proteins (9). ORF1a and ORF1b are translated into two polyprotein precursors that are further processed into 16 nonstructural proteins (nsp1 to nsp16). PEDV S protein binds to host receptor and mediates membrane fusion, initiating the infection process. Some cellular components in the cytoplasm, such as pattern recognition receptors (PRRs), function as sensors to detect and interact with viral pathogen-associated molecular patterns (PAMPs) to defend against infection. Interferons (IFNs) are secreted cytokines, and all three types of IFNs, types I (IFN-α, -β, and others), II (IFN-γ), and III (IFN-λ1, IFN-λ2, IFN-λ3, IFN-λ4), can activate a signal transduction cascade, leading to the expression of hundreds of interferon-stimulated genes (ISGs), and contribute to protecting the host from lethal viral infection (10–12). To evade the IFN system, which may block viral infection in multiple stages, coronaviruses (CoVs) have evolved various strategies to fight against it (13, 14). Among all 21 PEDV viral proteins, 11 proteins were found to be potential type III IFN antagonists, and 6 nsps inhibited IFN-β and interferon regulatory factor 3 (IRF3) promoter activities (15, 16). PEDV nsp1 was suggested to be the most potent IFN antagonist (15). Exogenous expression of PEDV nsp1 significantly suppressed both type I and type III IFN responses by interrupting the IRF3 and CREB-binding protein (CBP) association and suppressing transcription factors' activity. In addition, the residues N93 and N95 are crucial for type I and type III IFN suppression *in vitro* (15, 16). We hypothesized that a recombinant PEDV carrying mutations at the conserved residues N93 and N95 of nsp1 induces higher IFN responses and is more sensitive to IFN responses, leading to virus attenuation. To test this hypothesis, a recombinant PEDV N93/95A mutant carrying double alanine substitutions within the conserved motif (N93A and N95A) was designed and constructed. We characterized the viral growth kinetics, sensitivity to IFNs, and the induction of IFN responses in Vero and IPEC-DQ cells. Furthermore, we examined the pathogenicity and immunogenicity of this mutant in neonatal gnotobiotic (Gn) pigs.

RESULTS

The PEDV N93/95A mutant with engineered nsp1 was rescued using reverse genetics. Functional screening revealed that amino acids 91 to 95 of alphacoronavirus (α-CoV) nsp1 are crucial for its biological function (16). Sequence alignments showed that although CoV nsp1 has a low sequence identity between α-CoVs and β-CoVs, the N93 and N95 residues are highly conserved (Fig. 1A). Parental PEDV nsp1 and its counterpart with double alanine substitutions (N93A and N95A, designated the N93/95A mutant) were designed, and their structures were modeled using SWISS-MODEL (Fig. 1B). The recombinant PEDV N93/95A mutant was constructed based on the infectious clone (icPC22A) of a highly virulent PEDV strain, PC22A (17), and rescued in Vero cells. This virus was designated passage 0 (P0) of the N93/95A mutant. One clone of the mutant was selected by plaque purification and passaged once to generate the P1 virus stock. The complete genome of the N93/95A-P1 strain was verified by Sanger sequencing (Fig. 1C).

N93/95A mutant replicated less efficiently than icPC22A *in vitro*. First, we examined the effect of the nsp1 mutation on viral replication in cell cultures. The N93/95A mutant and its parental virus, the infectious clone-derived PC22A strain icPC22A, formed similar sizes of plaques (Fig. 2A). The multistep growth kinetics of the recombinant viruses was characterized in Vero and LLC-PK1 cells at a multiplicity of infection

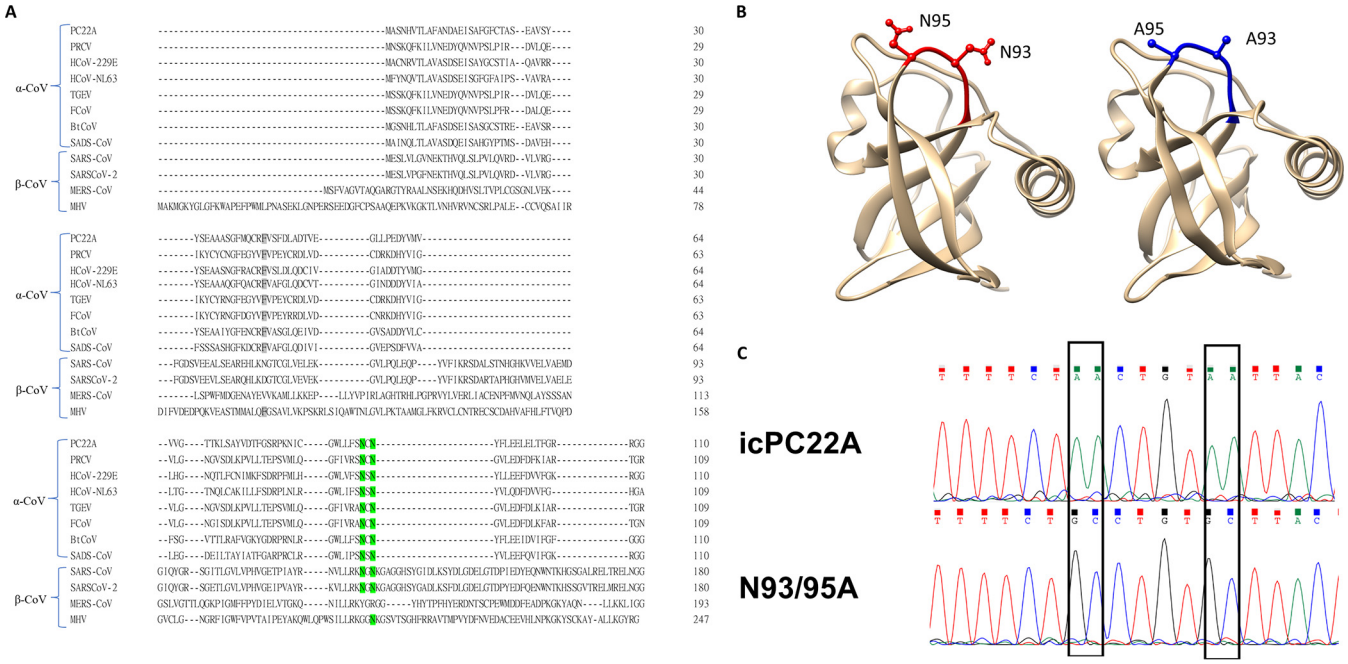

FIG 1 Generation of the icPC22A nsp1 N93/95A mutant. (A) Amino acid sequence alignment of nsp1 of α-CoVs (PEDV, TGEV, HCoV-NL63, HCoV-229E) and β-CoVs (MHV, MERS-CoV, SARS-CoV, SARS-CoV-2). PEDV nsp1 N93/N95 and the corresponding sites of other CoVs are labeled in green. PEDV nsp1 F44 and the corresponding sites of other CoVs are labeled in gray. (B) Predicted three-dimensional (3D) structure of PEDV nsp1 from icPC22A (left) and N93/95A mutant (right). The N93/N95 residues are shown in red, and the A93/A95 residues are shown in blue. (C) Sanger sequencing chromatogram of the N93A and N95A mutations shows the mutations were identified exclusively in the N93/95A mutant, but not in icPC22A.

(MOI) of 0.01. In both cells, the N93/95A mutant reached peak titers at approximately the same time as icPC22A. Although it replicated to titers of >5 $\log_{10}$ 50% tissue culture infective dose ($TCID_{50}$)/mL, its peak titers were significantly lower than those of the virulent icPC22A strain (Fig. 2B). Viral RNA production from the infected LLC-PK1 cells was evaluated using quantitative reverse transcription-PCR (RT-qPCR) (Fig. 2C). Subgenomic mRNAs (sgmRNAs) are mainly observed from actively replicating viruses, which directly function as the templates for the translation of structural and accessory proteins. Therefore, the expression levels of viral sgmRNAs are positively correlated with viral structural and accessory protein translation (18). LLC-PK1 cells infected with the N93/95A mutant had significantly lower viral sgmRNA/genomic RNA ratios than the cells infected with icPC22A (Fig. 2C). The reduced relative abundance of sgmRNA-3 or -N to genomic RNA in N93/95A strain-infected cells suggested a lower replication efficiency. To compare infectivity, we tested the infectious titers in median tissue culture infectious doses ($TCID_{50}$) and calculated the genomic RNA/$TCID_{50}$ ratios. The N93/95A mutant had significantly higher ratios than icPC22A (Fig. 2D). The highest ratio was observed at 24 h postinoculation (hpi) for the N93/95A mutant, indicating the significantly lower replication efficiency of the N93/95N strain than icPC22A at an early stage of infection. Although the replication efficiency of the N93/95A mutant increased as the infection process went on, it was always less than that of icPC22A ($P < 0.05$). Collectively, the N93/95A mutant showed decreased replication compared with icPC22A *in vitro*, and the modified nsp1 impaired virion infectivity in Vero and LLC-PK1 cells.

The N93/95A mutant was more sensitive to IFN pretreatment and induced stronger IFN responses than icPC22A *in vitro*. Since CoV nsp1 is a major antagonist to host IFN response, we compared the levels of replication of the N93/95A and icPC22A strains in Vero cells that were pretreated with different concentrations of IFNs (Fig. 3A to C). Type I (IFN-β) and type III (IFN-λ1 and IFN-λ3) IFNs inhibited the replication of both viruses in a dose-dependent manner. Compared with icPC22A, the N93/95A mutant was more sensitive to IFN-β at a concentration of 200 U/10^5 cells, to IFN-

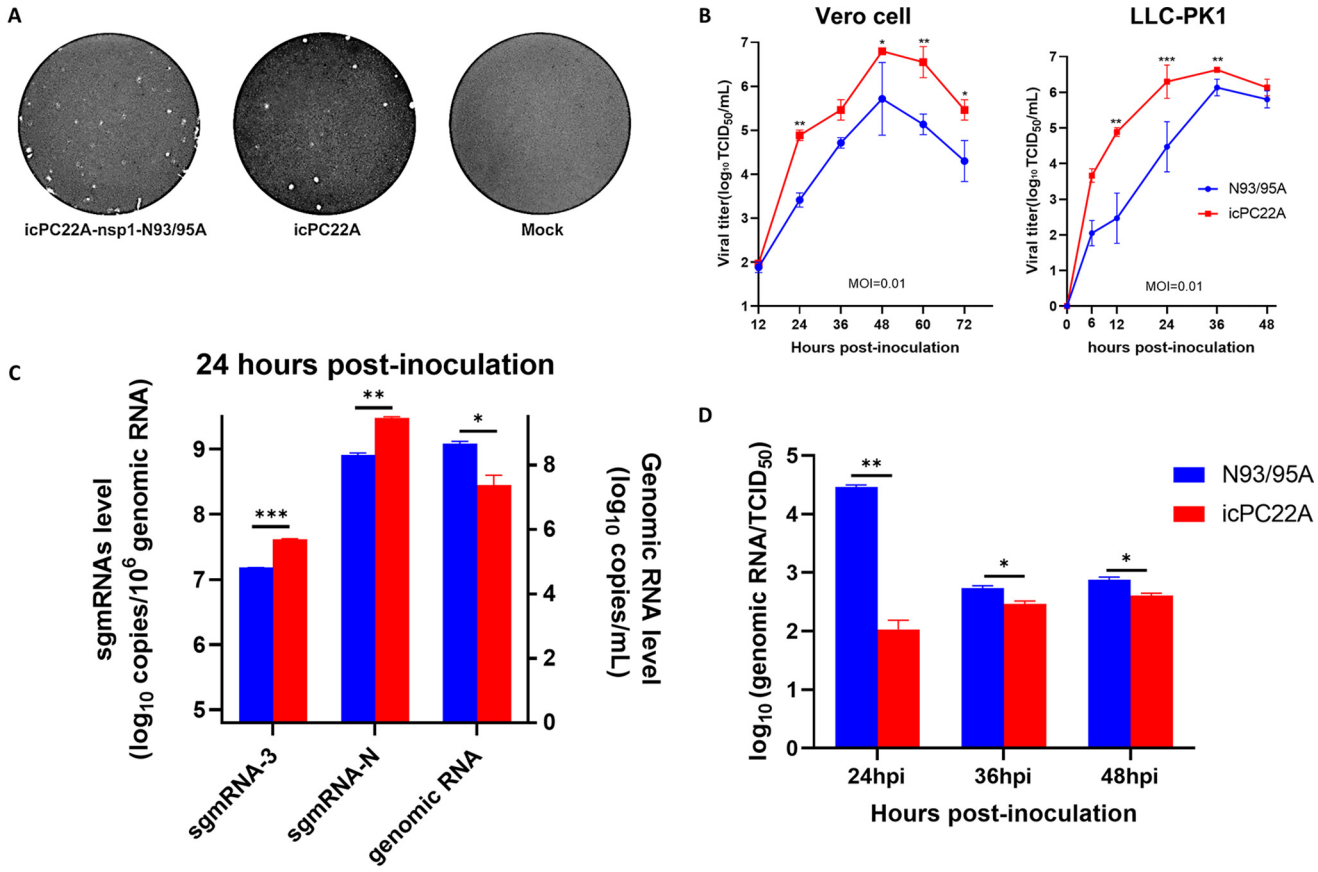

FIG 2 *In vitro* characterization of the N93/95A mutant. (A) Plaques of recombinant PEDVs in Vero cells. The mock-, N93/95A-, or icPC22A-infected cells were fixed and stained with crystal violet at 72 hpi. (B) Multistep growth curves of recombinant PEDVs (N93/95A mutant and the parental icPC22A strain) in Vero and LLC-PK1 cells at an MOI of 0.01. (C and D) LLC-PK1 cells were infected with the recombinant PEDV N93/95A or icPC22A strain at an MOI of 0.01. For panel C, cells were harvested at 24 hpi. The expression levels of sgmRNA-3 and sgmRNA-N (left *y* axis) and genomic RNA (right *y* axis) are presented. For panel D, we scratched cells from the plates and collected both cells and supernatant. Then, the samples were frozen and thawed for one cycle and centrifuged, and the supernatants were used for testing and calculation of the genomic RNA/$TCID_{50}$ ratios. Data from three replicates are shown as mean ± standard deviation (SD).

λ1 at less than 25 ng/mL, and to IFN-λ3 at less than 50 ng/mL. Because Vero cells are IFN deficient (19), we infected IPEC-DQ cells with icPC22A or the N93/95A mutant at an MOI of 3 and quantified the mRNA levels of swine IFN-β, IFN-λ1, and IFN-λ3 at 9 hpi (Fig. 3D to F) to evaluate whether the N93/95A mutant triggers enhanced type I and type III IFN responses in physiologically more relevant porcine intestinal cells. Compared with icPC22A, the N93/95A mutant induced significantly higher mRNA levels of all these IFNs at 9 hpi. In summary, these data suggested that the N93A and N95A mutations of PEDV nsp1 decreased viral antagonism to host type I and type III IFN responses in cell cultures.

The N93/95A mutant was partially attenuated in neonatal piglets. Five-day-old Gn pigs were inoculated orally (100 $TCID_{50}$/pig) with the N93/95A or icPC22A strain or mock inoculated and challenged with icPC22A at 22 days postinoculation (dpi) to investigate the pathogenesis and immunogenicity of the N93/95A mutant. All icPC22A-inoculated pigs (100% [5/5]) developed severe diarrhea from 1 dpi and died within 6 dpi (Fig. 4A and D). In comparison, although all N93/95A-inoculated piglets still had severe diarrhea, the onset of severe diarrhea was delayed. Only one pig of this group died (25% [1/4]) at 5 dpi. The virulent icPC22A-inoculated pigs shed peak PEDV RNA titers (11.71 ± 0.88 $\log_{10}$ copies/mL) in feces at 1.00 ± 0.00 dpi (Fig. 4B and Table 1). However, significantly diminished, and delayed PEDV fecal RNA peak shedding (9.77 ± 0.73 $\log_{10}$ copies/mL) was detected in N93/95A-inoculated pigs at 2.67 ± 1.03 dpi. For the infectious viral shedding, N93/95A-infected piglets showed significantly lower (4.80 ± 0.76 $\log_{10}$ $TCID_{50}$/mL) and delayed (at 2 dpi) peak

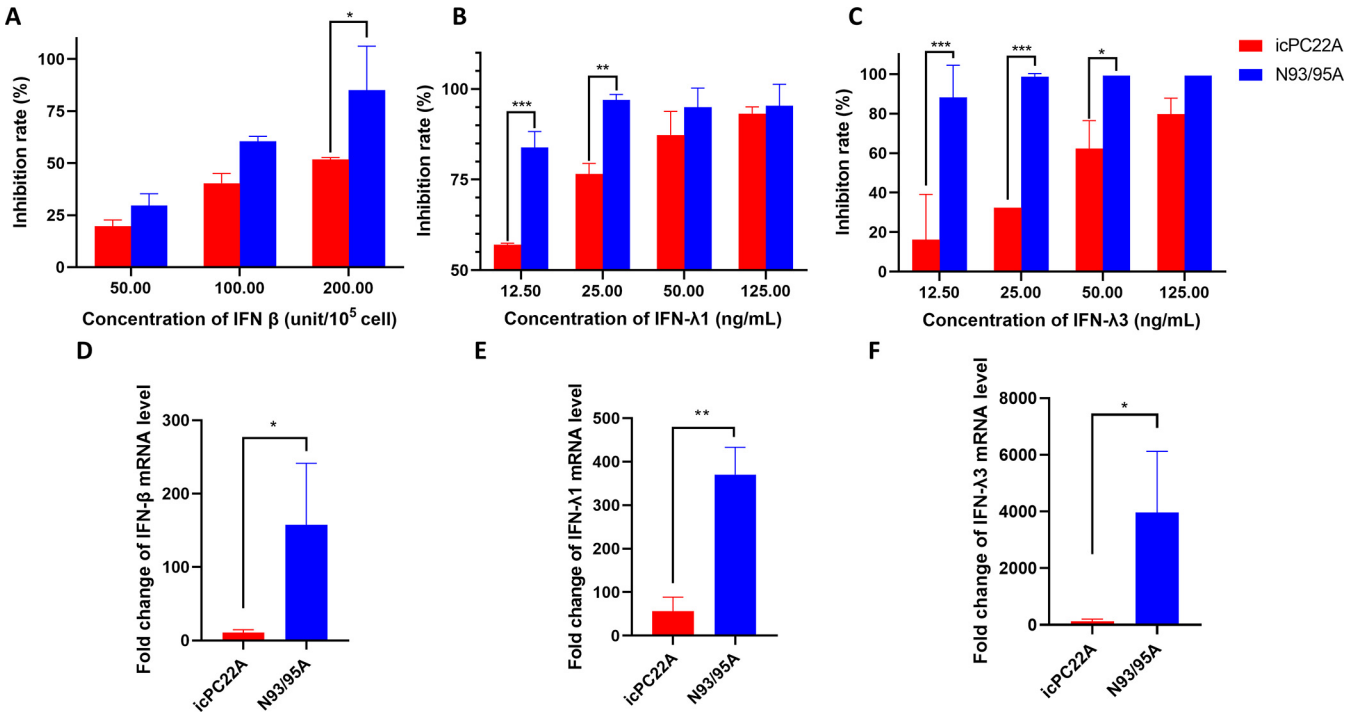

FIG 3 The N93/95A mutant exhibited impaired IFN antagonism compared with icPC22A. (A to C) Sensitivities of the recombinant PEDV N93/95A and icPC22A strains to IFN-β (A), IFN-λ1 (B), and IFN-λ3 (C) pretreatment of Vero cells. Cells were pretreated with different concentrations of IFNs and inoculated with the individual viruses at an MOI of 0.01 for 24 h. Supernatant and cells were collected and titrated for infectious virus titers in $TCID_{50}$. (D to F) Relative cellular mRNA levels of swine IFN-β, IFN-λ1, and IFN-λ3. IPEC-DQ cells were inoculated with recombinant PEDVs (MOI of 3) or mock inoculated. Total cellular RNA was extracted at 9 hpi and quantified by reverse transcription followed by real-time PCR. The values are fold changes compared with mock treatment using the $2^{-\Delta\Delta CT}$ method. Data from three replicates are shown as mean ± SD.

titers than the virulent icPC22A-inoculated pigs (5.80 ± 0.33 $\log_{10}$ $TCID_{50}$/mL at 1 dpi) (P = 0.0144) (Fig. 4C and Table 1). Infectious viral shedding was stopped at 5 dpi, although viral RNA shedding was detected until challenge from the N93/95A-inoculated pigs. Immunohistochemical (IHC) staining showed extensive PEDV N protein staining in the remaining epithelial cells of small intestines of pigs in the icPC22A and N93/95A groups (Fig. 4D). The villous height/crypt depth (VH/CD) ratios of the icPC22A-infected pigs were significantly lower than those of the N93/95A infected pigs, indicating that icPC22A induced more severe villous atrophy in jejunum than N93/95A (Fig. 4E). Collectively, these data suggest that the N93/95A mutant was partially attenuated in neonatal piglets.

N93/95A mutant induced partial protection against virulent icPC22A challenge in pigs. At 22 dpi, all remaining pigs were challenged with the highly virulent icPC22A strain at a high dose (10^6 PFU/pig) (Table 2). Following challenge, no mortality was observed in the N93/95A group, whereas one mock-challenged pig died at 8 days postchallenge (dpc), which was consistent with our previous reports that PEDV causes low mortality in older pigs (17). By 9 dpc, pigs in the N93/95A group only had mild diarrhea for 3.67 ± 0.58 days. However, all of the mock-challenged pigs (100% [4/4]) developed severe diarrhea for 6.00 ± 0.82 days. Also, pigs in the N93/95A group exhibited significantly lower peak PEDV RNA shedding titers (5.57 ± 0.89 $\log_{10}$ copies/mL) than the pigs in the mock-challenged group (9.98 ± 0.93 $\log_{10}$ copies/mL) (P = 0.0010) (Fig. 5C and Table 2). Although very low levels of viral RNA shedding were detected from the N93/95A group, only pigs in the mock-challenged group had infectious viral shedding from 2.67 ± 0.58 days, but not the pigs in the N93/95A group after virulent PEDV challenge (Fig. 5B and C and Table 2). Viral neutralization (VN) antibody titers in the sera collected at 14 dpi, 22 dpi/0 dpc, and 31 dpi/9 dpc were determined by plaque reduction viral neutralization assay (Fig. 5C). Primary infection of piglets with the N93/95A mutant elicited VN antibodies to a geometric mean titer (GMT) of 508.0 before challenge (at 22 dpi/0 dpc), and the challenge significantly boosted the VN titer (GMT,

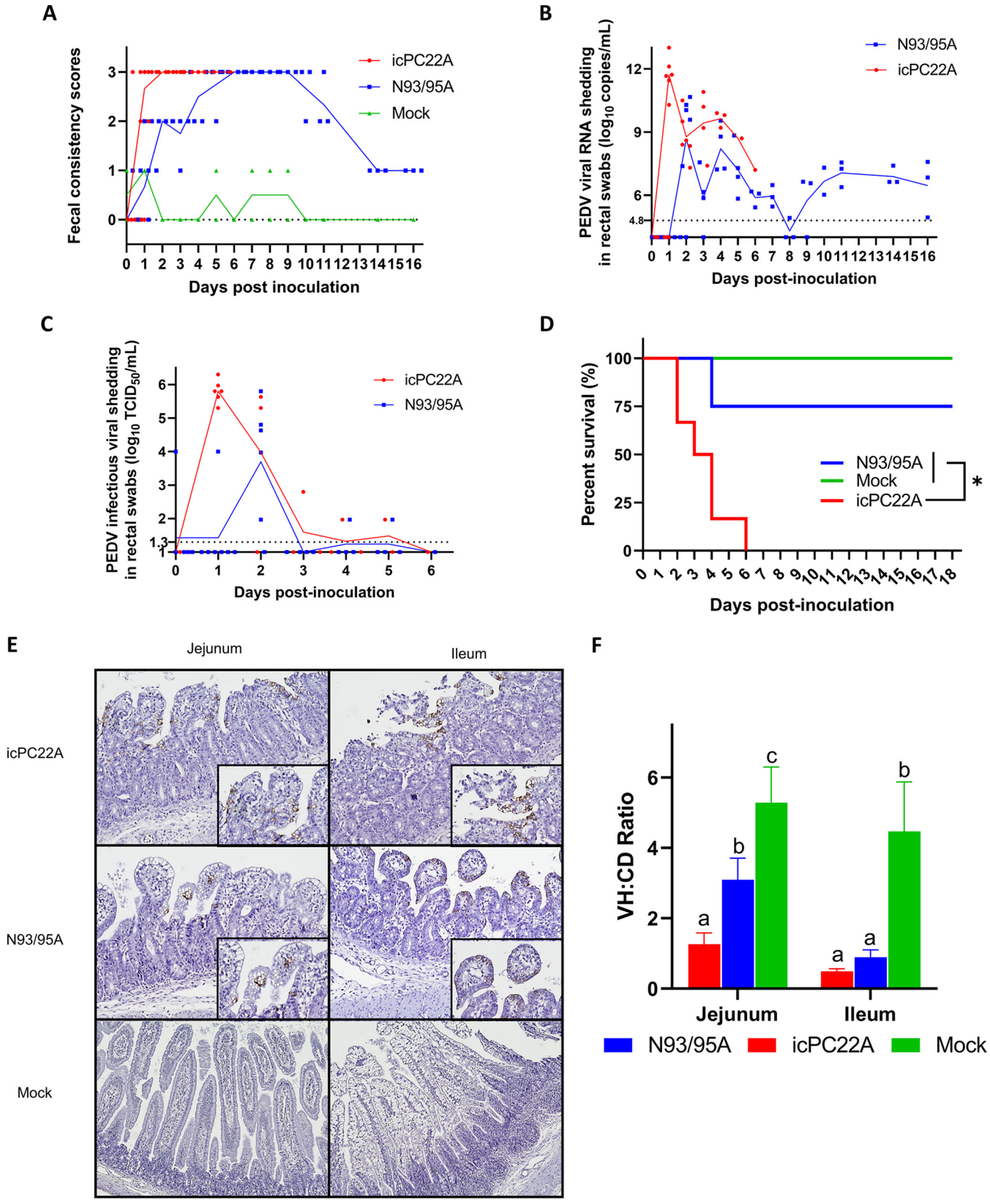

FIG 4 Pathogenicity of the recombinant PEDV N93/95A and icPC22A strains in Gn piglets. (A) Fecal consistency scores of pigs from preinoculation to 16 dpi. Fecal consistency was scored as follows: 0, solid; 1, pasty; 2, semiliquid; and 3, liquid. Each dot represents the score of an individual pig; each line indicates the mean score of a group. Scores of ≥2 and 3 were considered diarrhea and severe diarrhea, respectively. All pigs in the icPC22A group died by 6 dpi. (B) PEDV RNA (N gene) shedding titers in rectal swabs from preinoculation to 16 dpi. Each symbol represents the titer of an individual piglet; each

(Continued on next page)

TABLE 1 Summary of clinical signs and fecal PEDV shedding of Gn piglets at 1 to 21 days after PEDV inoculation

Group	No. of pigs[a]	Mortality rate, % (no./total)	Severe diarrhea rate, % (no./total)[b]	Onset of diarrhea (dpi)[b]	Peak mean infectious shedding titer (log_{10} $TCID_{50}$/mL)	Peak mean RNA shedding titer (log_{10} N gene copies/mL)
icPC22A	6	100 (5/5) A[c]	100 (5/5)	1.00 ± 0.00 A	5.80 ± 0.33 A (1 dpi)	11.71 ± 0.88 A (1 dpi)
N93/95A	6	25 (1/4) B	100 (4/4)	2.00 ± 0.00 B	4.80 ± 0.76 B (2 dpi)	9.77 ± 0.73 B (2 dpi)
Mock inoculated	5	0 (0/4)	0 (0/4)	NA[d]	NA	NA

[a]One pig each from the icPC22A- and mock-inoculated groups and two pigs from the N93/95A mutant-inoculated group were euthanized at 3 dpi for histopathological examination and were excluded for the calculation of mortality and diarrhea rates, peak mean RNA shedding titers, and onset of peak RNA shedding.
[b]Fecal scores of 2 and 3 were considered moderate diarrhea and severe diarrhea, respectively.
[c]Different letters denote significant difference between groups ($P < 0.05$).
[d]NA, not available.

1,015.9 at 31 dpi/9 dpc), which was significantly higher than that (100.8) of the mock-challenged group. In summary, N93/95A infection of 5-day-old piglets induced VN antibody response and 100% protection against severe diarrhea and death following challenge with virulent icPC22A.

The N93/95A mutant was genetically stable after serial passaging *in vitro* and *in vivo*. Reversion to virulence is one of the major concerns for live attenuated vaccines. To evaluate the genetic stability of the mutant, the N93/95A-P1 strain was serially passaged in three independent lineages in Vero cells nine times to the N93/95A-P10 strain (Fig. 6A). Whole genomic sequences were determined for the three lineages of the N93/95A-P10 strain by Sanger sequencing. Across the three lineages of the N93/95A-P10 strain, there were no reversion mutations observed in the A93 and A95 residues. Also, no additional mutations were acquired by PEDV nsp1 during serial passaging in Vero cells. Analysis of the entire genomes identified two nonsynonymous mutations in nsp3 from lineage 1 (L1293S) and lineage 3 (E152Q) (Fig. 6B). Meanwhile, we evaluated the genetic stability of the mutant confronting the selective pressure in the pig intestines by sequencing PEDV genomes in the rectal swab samples collected from Gn pigs. Swabs from the N93/95A strain-infected pigs collected at 2 to 11 dpi revealed no reversion mutation at the A93 and A95 sites. However, due to relatively low viral RNA titers in the swabs, we failed to sequence the whole genomes from them. Collectively, the results from passaging the N93/95A mutant in either cell culture or piglets revealed the N93A and N95A mutations were genetically stable.

DISCUSSION

Several deadly human or animal CoVs have emerged or reemerged in the past 2 decades, such as severe acute respiratory syndrome associated coronavirus (SARS-CoV), Middle East respiratory syndrome coronavirus (MERS-CoV), SARS-CoV-2, PEDV, porcine deltacoronavirus (PDCoV), and swine acute diarrhea syndrome coronavirus (SADS-CoV) (20–24). Vaccination is expected to be an efficacious strategy in preventing individuals and animals from suffering from CoV diseases. As for the control and prevention of PEDV, the U.S. Department of Agriculture has conditionally licensed two vaccines to induce immunity in pregnant sows that can provide passive protection in piglets via colostrum and milk: an inactivated virus vaccine (Zoetis, Inc.) and a Venezuelan equine encephalitis virus (VEEV)-vectored vaccine carrying the PEDV S gene (Merck & Co., Inc.). However, neither vaccine can induce sufficient lactogenic immunity in PEDV-naive sows to protect piglets from PED (25, 26). Live attenuated vaccines (LAVs) administered orally can replicate robustly in the gut, mimic natural infection, and induce both local mucosal and systemic immune responses. Oral inoculation of live attenuated PEDV to seronegative pregnant sows can

FIG 4 Legend (Continued)
line indicates the mean value from a group. The dashed line at 4.8 log_{10} copies/mL indicates the detection limit. (C) Fecal infectious PEDV titers of pigs postinoculation. Each symbol represents the titer of an individual piglet; each line indicates the mean value from a group. The dashed line at 1.3 log_{10} $TCID_{50}$/mL indicates the detection limit. (D) Survival curves of pigs after inoculation with N93/95A or icPC22A by 18 dpi. (E) Immunohistochemistry staining of PEDV N proteins in jejunum and ileum sections from piglets euthanized at 3 dpi (magnification, ×100). (F) VH/CD ratios for piglets. Ten villi of each intestinal section were measured. Data are shown as mean ± SD. Groups with significant differences ($P < 0.05$) are indicated with different letters.

TABLE 2 Clinical signs and PEDV shedding of pigs at 1 to 9 days postchallenge with the highly virulent icPC22A strain

Group	No. of pigs	Mortality rate, % (no./total)	Severe diarrhea rate, % (no./total)[a]	Duration of severe diarrhea (days)[a]	Duration of diarrhea (days)[a]	Peak mean RNA shedding titer (log_{10} N gene copies/mL)
N93/95A	3	0 (0/3)	0 (0/3) A[b]	0.00 ± 0.00 A	3.67 ± 0.58 A	5.57 ± 0.89 A
Mock inoculated	4	25% (1/4)	100 (4/4) B	6.00 ± 0.82 B	7.25 ± 1.50 B	9.98 ± 0.93 B

[a]Fecal scores of 2 and 3 were considered moderate diarrhea and severe diarrhea, respectively.
[b]Different letters denote significant difference between groups ($P < 0.05$).

reduce the mortality of neonatal pigs more effectively than intramuscular injection of an inactivated vaccine (27).

The CoV nsp1 has been reported as a potential host IFN antagonist (16, 28). It is found in α-CoVs and β-CoVs among the four CoV genera and is considered a genus-specific marker (29, 30). Although there is low sequence identity between the nsp1 proteins of α-CoVs and β-CoVs, a relatively conserved domain was identified in the core structure (31–33). Corresponding to the similar structure, nsp1 proteins of α-CoVs and β-CoVs exhibit remarkably similar biological functions. CoV nsp1 inhibition of host gene expression has been well characterized for SARS-CoV, a member of β-CoV: (i) SARS-CoV nsp1 binds to the 40S ribosomal subunit and inactivates its translation function, and (ii) the nsp1-40S complex contributes to the endonucleolytic cleavage of host mRNAs (34, 35). It is also evident that SARS-CoV nsp1 suppresses host antiviral signaling pathways and antagonizes host innate immunity by inhibiting IFN expression (36, 37). Previous studies of MERS-CoV, another β-CoV, revealed that its nsp1 exhibited similar activities in suppressing host gene expression. Alanine substitutions of critical residues (K181A or R125A/K126A) in MERS-CoV nsp1 abolished its biological function (38). As we enter the third year of the COVID-19 pandemic, SARS-CoV-2 is spreading between people at an intense level globally. The nsp1 of SARS-CoV-2 is considered one host shutoff factor because it can suppress host gene expression. It interacts with the 40S subunit in a ribosomal complex and inserts its C terminus, bearing residues N126 and N128 (with N93 and N95 the corresponding residues in SARS-CoV-2), into the mRNA

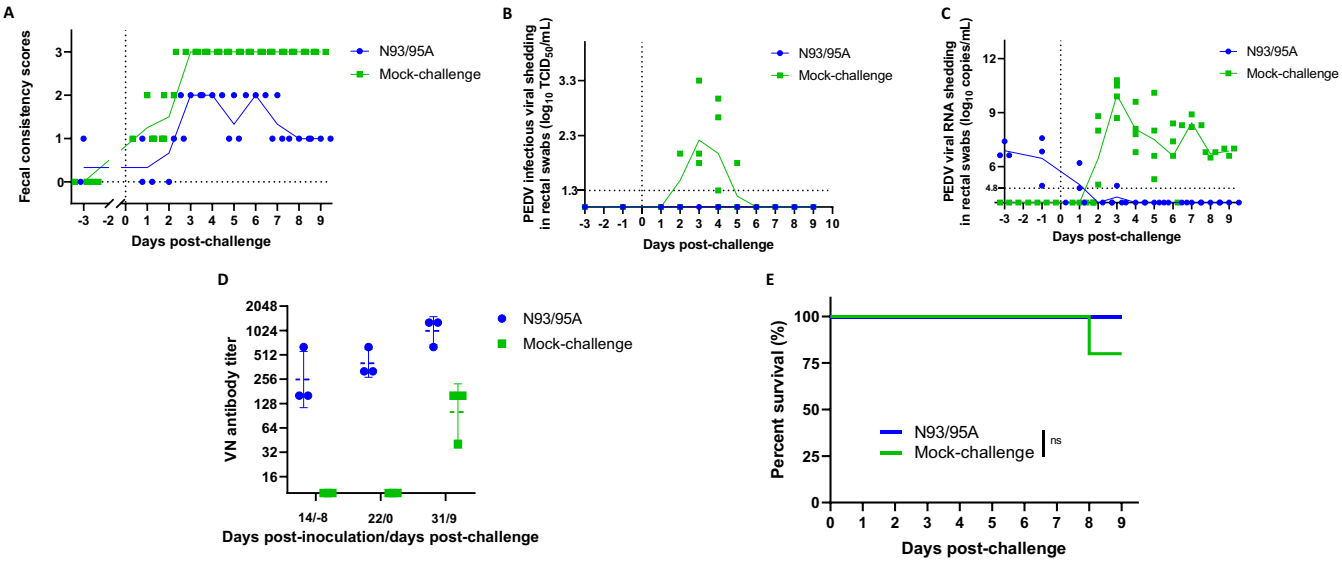

FIG 5 Induction of partial protection by the N93/95A mutant in Gn pigs against icPC22A challenge. (A) Fecal consistency scores of pigs postchallenge. Fecal consistency was scored as follows: 0, solid; 1, pasty; 2, semiliquid; and 3, liquid. Scores of ≥2 and 3 were considered diarrhea and severe diarrhea, respectively. Each dot represents the score of an individual pig; each line indicates the mean score of a group. (B) Fecal infectious PEDV titers of pigs postchallenge. Each symbol represents the titer of an individual piglet; each line indicates the mean value of a group. The dashed line at 1.3 log_{10} $TCID_{50}$/mL indicates the detection limit. (C) PEDV RNA (N gene) shedding titers in rectal swabs postchallenge. Each symbol represents the titer of an individual piglet; each line indicates the mean value of a group. The dashed line at 4.8 log_{10} copies/mL indicates the detection limit. (D) VN antibody titers in serum samples collected at different time points. Each symbol represents the titer of an individual piglet. Data are shown as mean ± SD. (E) Survival curves of pigs by 9 dpc.

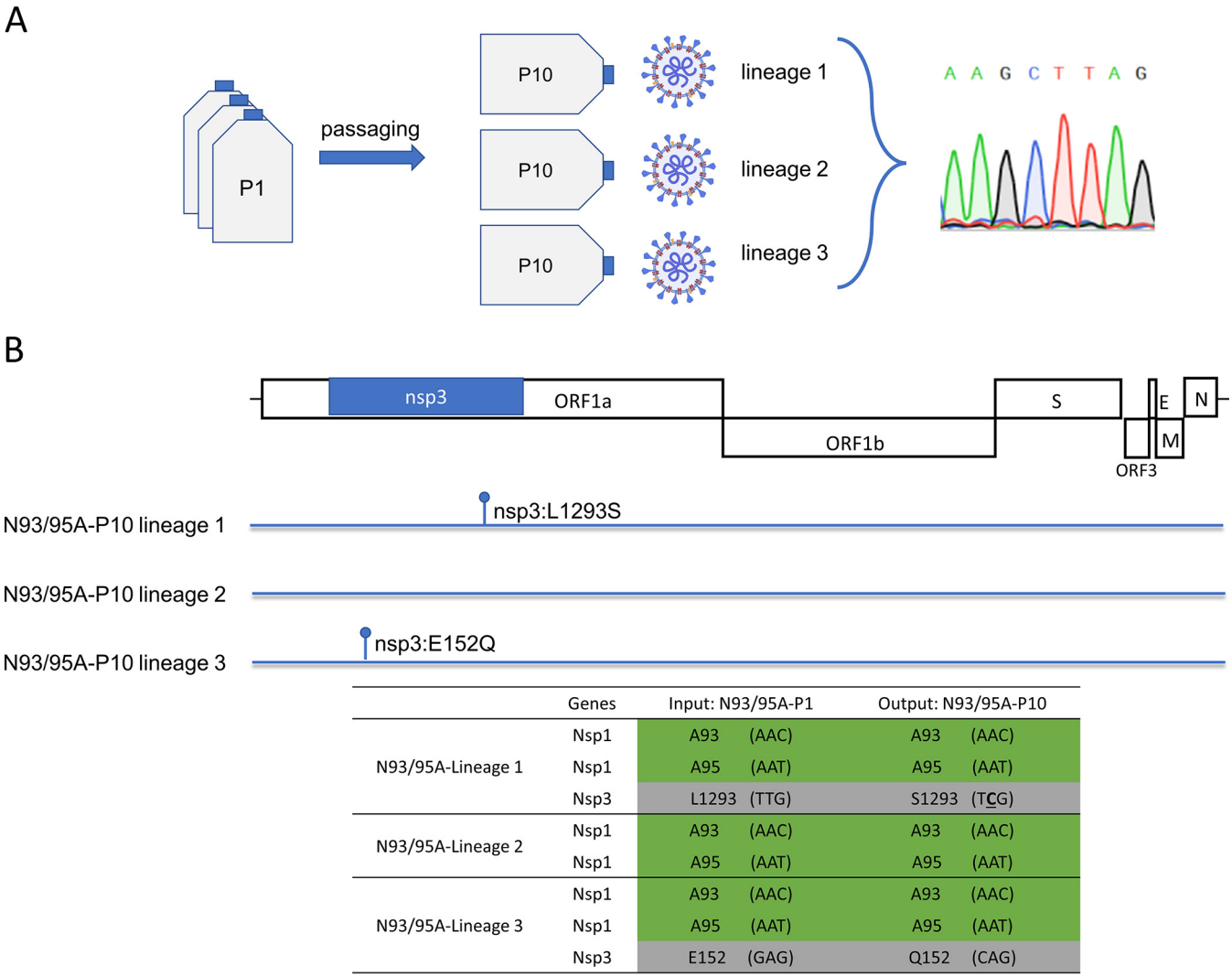

	Genes	Input: N93/95A-P1	Output: N93/95A-P10
N93/95A-Lineage 1	Nsp1	A93 (AAC)	A93 (AAC)
	Nsp1	A95 (AAT)	A95 (AAT)
	Nsp3	L1293 (TTG)	S1293 (TCG)
N93/95A-Lineage 2	Nsp1	A93 (AAC)	A93 (AAC)
	Nsp1	A95 (AAT)	A95 (AAT)
N93/95A-Lineage 3	Nsp1	A93 (AAC)	A93 (AAC)
	Nsp1	A95 (AAT)	A95 (AAT)
	Nsp3	E152 (GAG)	Q152 (CAG)

FIG 6 Genetic stability of the N93/95A mutant. (A) Scheme of evaluation of the genetic stability of the N93/95A mutant in Vero cells; (B) summary of identified mutations and substitutions of interest in the N93/95A-P1 (input) and N93/95A-P10 (output) strains.

channel, interfering with mRNA binding. Moreover, nsp1 inhibits nuclear export of cellular mRNA by binding mRNA export receptor NXF1. Therefore, SARS-CoV-2 nsp1 plays a central role in global inhibition of translation, including IFN responses (39–42). In terms of α-CoV nsp1, transient gene expression was widely employed to elucidate its biological function and the key residues in that process (15, 16, 43). Shen et al. suggested that the expression of a reporter gene was significantly inhibited upon transient expression of nsp1 from several representative α-CoVs, including PEDV, transmissible gastroenteritis virus (TGEV), human coronavirus 229E (HCoV-229E), human coronavirus NL63 (HCoV-NL63), and feline infectious peritonitis virus (FIPV) (43). A conserved motif (amino acids 91 to 95) was characterized in TGEV. A recombinant TGEV with disrupted 91–95 motif showed comparable replication to parental virus *in vitro* but exhibited an attenuated phenotype in the pig model (43). Like our study, Deng et al. targeted nsp1 for PEDV attenuation. They generated one nsp1 F44A mutant that induced increased mRNA levels of IFN-β and IFN-λ1 upon infection of LLC-PK1 cells (44). In this study, we engineered amino acid sites N93A and N95A instead of F44A because N93 and N95 residues are more conserved among α-CoVs and β-CoVs than the F44 residue. The infection of the icPEDV Nsp1 mutant carrying F44A induced slightly increased IFN and ISG54 mRNA expression level. However, the pathogenicity of the F44A mutant was not evaluated in pigs. Therefore, it is hard to illustrate the role of nsp1 in PEDV virulence. In the present study, the N93/95A mutant triggered a significantly higher

IFN mRNA level and was more sensitive to IFN pretreatment in cell culture. Meanwhile, it was attenuated and induced 100% protection against severe diarrhea and death postchallenge in neonatal Gn pigs. In addition, the N93A and N95A mutations were genetically stable. All of these facts make them ideal targets for a LAV. In addition to the nsp1 N93 and N95, we previously identified several virulence-determining mutations, including the endocytosis signal of the S protein and the catalytic sites KDKE of nsp16 2′-*O*-methyltransferase, as potential LAV targets (17, 45). Further investigation is needed to test the immunogenicity of the LAV candidates carrying different combinations of these targeted mutations in sows, which can generate immune responses and passively protect the nursing piglets from the highly virulent PEDV infection via colostrum and milk. Interestingly, our data suggested that even in IFN-deficient Vero cells, the N93/95A mutant exhibited impaired replication compared with icPC22A. It suggested that in addition to functioning as an IFN antagonist, PEDV nsp1 may promote viral replication via other mechanisms. For example, in CoVs, including PEDV, nsp1 can inhibit general host gene expression to support viral protein translation using the host machinery (33, 43). We observed decreased sgmRNA levels for the N93/95A mutant compared with virulent icPC22A. This could be due to the lower level of viral protein translation in the nsp1 mutant-infected cells, and this hindered virion assembly and the following virion release, resulting in an increased level of viral genomic RNA inside the infected cells and low infectious titers at 36 hpi (Fig. 2B). Thus, the increased genomic RNA in cytoplasm led to a relatively low sgmRNA/genomic RNA ratio in nsp1 mutant-infected cells (Fig. 2C). Collectively, we determined that the nsp1 gene is a virulence-determining gene of PEDV by evaluating the N93/95A mutant both *in vitro* and *in vivo*.

Emerging and reemerging zoonotic CoVs have constantly crossed species barriers and posed an extraordinary threat to global public health for the past 2 decades. Up to date, there are seven human CoVs (HCoVs) known to be zoonotic: HCoV-229E, HCoV-NL63, HCoV-OC43, HCoV-HKU1, SARS-CoV, MERS-CoV, and SARS-CoV-2 (46–53). Most recently, novel canine-feline recombinant α-CoVs and PDCoV were detected from humans (54–56). Although no zoonotic transmission has been reported for PEDV, SADS-CoV showed potential zoonotic risk (57). Pigs, as a major livestock animal, may serve as a mixer for virus recombination, which contributes to the emergence of novel zoonotic CoVs. In the current study, we provided promising mutagenesis sites, nsp1 N93 and N95A, for LAV development not only for PEDV, but also for other human and animal α-CoVs and β-CoVs.

The innate immune system is the first line of host defense against invading pathogens. IFNs are soluble glycoproteins with strong antiviral activities first identified in 1957 and classified into three types: I, II, and III (58). Virus-infected cells secret IFN-α and IFN-β, which bind to type I-specific receptors on adjacent cells and activate those cells to an antiviral state. IFN-λs are type III IFNs, which mainly function in epithelium-derived cells and are recognized as a key player in innate mucosal immunity. PEDV infects mainly small intestinal villous enterocytes and can be suppressed by local mucosal immune responses (21, 59). We found that the N93/95A mutant triggered robust type I and type III IFN responses *in vitro*. Beyond that, we also demonstrated that the N93/95A strain was more sensitive to type I and type III IFN pretreatment in cell cultures. The significantly increased genomic RNA/$TCID_{50}$ ratio at 24 to 48 hpi suggested that the N93/95A mutant was less efficient at establishing productive infection at the early stage than the parental virus. In addition to the innate immunity, VN antibodies were tested to provide information on PEDV-specific protective immunity responses. The primary infection of N93/95A elicited significant VN antibodies at 14 dpi, and this was boosted by virulent strain challenge, suggesting that the immunogenicity of the N93/95A mutant was retained. Our results suggest that nsp1 N93 and N95 residues are good targets for the design of PEDV LAVs. Because N93 and N95 are conserved among the nsp1 proteins of α-CoVs and β-CoVs, they may also be the targets for the development of LAVs for future emerging α-CoVs and β-CoVs.

MATERIALS AND METHODS

Cells and reagents. Vero cells (ATCC no. CCL81) were cultured in Dulbecco's modified Eagle's medium (DMEM) (Life Technologies, Carlsbad, CA) in the presence of 5% fetal bovine serum (FBS) (HyClone,

Logan, UT), and antibiotics and antimycotic (100 U/mL penicillin, 100 μg/mL streptomycin, and 250 ng/mL amphotericin B) (Life Technologies, Carlsbad, CA) (60). LLC porcine kidney (LLC-PK1) cells (ATCC CL-101) were cultured in modified Eagle's medium (MEM) supplemented with 5% fetal bovine serum (FBS), 1% nonessential amino acids (NEAA), 1% antibiotic–antimycotic, and 1% HEPES. IPEC-DQ cells, a subline of IPEC-J2 cells, were maintained in RPMI 1640 supplemented with 10% FBS (16). After being inoculated with PEDV, Vero cells were maintained in DMEM supplemented with 0.3% tryptose phosphate broth (TPB) (Life Technologies, Carlsbad, CA), antibiotics (100 U/mL penicillin and 100 μg/mL streptomycin) (Life Technologies, Carlsbad, CA), and 10 μg/mL trypsin (Life Technologies, Carlsbad, CA) as described previously (17), LLC-PK1 cells were maintained in MEM supplemented with 1% antibiotic–antimycotic, 1% NEAA, 1% HEPES, and 10 μg/mL trypsin, and IPEC-DQ cells were maintained in RPMI 1640 containing 0.3% TPB, 1% penicillin–streptomycin and 1 μg/mL trypsin (16).

Structural modeling and sequence alignment. The three-dimensional structural modeling of the nsp1 of the PEDV icPC22A and N93/95A mutant strains was performed at SWISS-MODEL (https://swissmodel.expasy.org) using template 5xbc.1.A. The structural analysis was carried out with UCSF Chimera (http://www.rbvi.ucsf.edu/chimera). Sequence analysis and alignment were performed using DNAStar Lasergene software.

Generation of recombinant PEDV with mutated nsp1. The PEDV mutant carrying mutations in nsp1 (Fig. 1C) was subjected to recovery based on the full-length cDNA clone of PEDV strain PC22A as described previously (17). The point mutations were introduced into the plasmid pUC19 carrying fragment A of icPC22A via the NEB Q5 site-directed mutagenesis kit (NEB, Ipswich, MA). Then, the insertion sequences of plasmids were confirmed by Sanger sequencing. After the plasmids were digested by restriction enzymes, the appropriately sized cDNA inserts were purified using the QIAquick gel extraction kit (Qiagen, Hilden, Germany). All five fragments (A, B, C, D, and E) were ligated with T4 ligase (NEB, Ipswich, MA) at 4°C overnight in an equal molar ratio for full-length cDNA. The ligated full-length cDNAs were purified by chloroform extraction and used as the templates for *in vitro* transcription using an mMessage mMachine T7 transcription kit (Ambion, Austin, CA). The polyadenylated PEDV N gene transcript was generated with an inserted T7 promoter and coelectroporated into Vero cells with the full-length transcripts at 450 V and 50 μF using a Gene Pulser II electroporator (Bio-Rad, Hercules, CA). At 18 h after electroporation, the growth medium was discarded, and Vero cells were cultured in maintenance medium in the presence of 10 μg/mL trypsin. Cells were monitored for cytopathic effect (CPE) and harvested—designated P0 virus. The P0 virus was subjected to plaque purification, and one clone was propagated to generate the P1 stock for the mutant. The full genome of the P1 virus stock was confirmed by Sanger sequencing.

Plaque assay and $PRNT_{50}$. For the plaque assay, monolayers of Vero cells in six-well plates were inoculated with virus serially diluted 10-fold for 1 h in the presence of trypsin. Fifty percent plaque reduction neutralization titers ($PRNT_{50}$s) were determined as described previously, with modifications (61). Briefly, 4-fold serially diluted serum samples were mixed with equal volumes of PEDV, and the serum-virus mixtures were incubated at 37°C for 90 min. A virus control (50 PFU of virus/well for the final inoculation), medium control, and positive and negative serum controls were included. The cell monolayers were washed and inoculated with the serum-virus mixtures or controls. Each sample was duplicated. The plates were incubation at 37°C for 1 h. After incubation, the inoculum was removed, and cells were washed with phosphate-buffered saline [PBS(−)] (Life Technologies, Carlsbad, CA). Then, cell monolayers were covered with 2 mL/well of overlay containing 1.5% agarose in MEM supplemented with 10 μg/mL trypsin and 0.3% TPB. At 3 dpi, the cells were fixed with 10% PBS-buffered formalin for 15 min and stained with 0.2% crystal violet. The VN titer of a serum sample was defined as the reciprocal of the highest dilution that reduced at least 50% of the plaques based on the virus control wells.

Multistep growth kinetics for PEDV. Vero or LLC-PK1 cell monolayers in six-well plates were inoculated with the corresponding viruses at an MOI of 0.01. After 1 h of adsorption, the virus inoculum was removed, and the cells were washed with PBS(−) to remove the unbound virions and cultured in maintenance medium at the presence of trypsin. Both cells and supernatants were collected at multiple time points and titrated for infectivity in 96-well plates for $TCID_{50}$ by the Reed-Muench method (62). Then, the same samples were quantified for genomic RNA as previously described (17) to calculate the genomic RNA/$TCID_{50}$ ratio. Because sgmRNAs are mainly found in cells with actively replicating viruses, only LLC-PK1 cell layers infected with icPC22A or the N93/95A mutant at an MOI of 0.01 were harvested at 24 hpi and subjected to total RNA extraction using TRIzol reagent (Invitrogen, Carlsbad, CA) to quantify the sgmRNAs and genomic RNA. The cellular DNA was removed by treating the RNA with DNase I (Qiagen). Five hundred nanograms of RNA was used for sgmRNAs and genomic RNA detection (17). sgmRNA-3 was amplified with a forward primer (5′-CTATCTACGGATAGTTAGCTC-3′) targeting the leader-body junction sequences, a reverse primer (5′-CTGTGTCAATCGTGTATTG-3′), and a probe (5′-6-carboxyfluorescein [FAM]-ACATCACTGCACGTGGAC-black hole quencher [BHQ]-3′). sgmRNA-N was amplified with a forward primer (5′-CTCTTGTCTACTCAATTCA ACTAAACAGAAAC-3′) targeting the leader-body junction sequences, a reverse primer (5′-CCAGTATCCAATTT GCTGGTCC-3′), and a probe (5′-FAM-TCAGGATCGTGGCCGCAAAC-BHQ-3′). The genomic RNA was amplified with a forward primer (5′-TGAAGCCGTCTCATACTATTCTG-3′), a reverse primer (5′-AATCCCTCAACAGT GTCAGC-3′), and a probe (5′-FAM-TGCAATGCCGTTTCGTGTCCTTC-BHQ-3′) targeting the nsp1 gene (17). Copy numbers of each were determined by standard curves.

IFN sensitivity assay. Vero cells were cultured in medium supplemented with different concentrations of type I (IFN-β) (R&D Systems, Inc., Minneapolis, MN) and type III (IFN-λ1 and -λ3) (PBL Assay Science, Piscataway, NJ) IFNs for 18 h prior to PEDV inoculation as previously described (17). After removal of the medium and washing the cells with PBS(−) three times, the cells were inoculated with recombinant PEDVs at an MOI of 0.01 and cultured for an additional 24 h. The supernatants and cells

were frozen at −80°C. After freezing and thawing once, the samples were centrifuged, and the supernatants were collected and titrated by $TCID_{50}$. The inhibition rate was calculated as follows: inhibition rate = [(titer of viral control − titer of virus in IFN-pretreated cells)/titer of viral control] × 100%.

Interferon induction assay. IPEC-DQ cells were inoculated with recombinant PEDVs at an MOI of 3. After the 1-h adsorption, the virus inoculum was removed, and the cells were washed with PBS(−). At 9 hpi, the supernatants were removed, and the total cellular RNA was extracted with TRIzol reagent (Invitrogen, Carlsbad, CA). Then, cellular DNA was removed by treating the extracted RNA with DNase I (Qiagen). One microgram of total RNA was reverse transcribed using Moloney murine leukemia virus (MMLV) reverse transcriptase and random primers (Promega, Madison, WI). The cDNA was subjected to quantitative PCR using SYBR green PCR mix (Life Technologies, Carlsbad, CA) according to the manufacturer's instructions. Primers for IFN detection were described previously (15). The β-actin gene was used as an internal control. The threshold cycle (C_T) values for target genes and the differences in their C_T values (ΔC_T) were determined. Relative transcription levels of target genes are presented as fold changes relative to the respective controls using the $2^{-\Delta\Delta CT}$ method (63).

Study of the pathogenesis and immunogenicity of the recombinant PEDVs in Gn pigs. All experiments carried out in this study were approved by the Institutional Animal Care and Use Committee (IACUC) of The Ohio State University. Gn pigs were delivered from PEDV-free sows via C-section. At 5 days of age, Gn piglets were orally inoculated with 100 $TCID_{50}$/pig of the N93/95A mutant (E191A-P1) ($n = 6$) or icPC22A ($n = 6$) or were mock inoculated with ($n = 5$). In our lab, we titrate PEDV using plaque assay for PFU and/or microwell assay for $TCID_{50}$, and the titers are similar using these two methods for PEDV PC22A. So, this inoculation dose of PEDV corresponds to a value of 100 to 1,000 of the 50% porcine diarrhea dose (PDD_{50}) of the PC22A strain in 4-day-old cesarean-derived, colostrum-deprived piglets (64). One piglet in the icPC22A group, one pig in the mock-inoculated group, and two pigs in the N93/95A group were euthanized at 3 dpi for histopathological examinations. At 22 dpi, each pig was challenged orally with 6 $\log_{10}$ PFU of icPC22A and was monitored for 9 days before euthanasia. This high challenge dose mimics the infectious dose in the field and was used in our previous PEDV studies with similar ages of pigs (17, 45, 65). After virus inoculation, clinical signs, including diarrhea and vomiting, were monitored daily. Rectal swabs were collected daily. The severity of diarrhea was scored based on the fecal consistency (FC) in individual pigs: 0, solid; 1, pasty; 2, semiliquid (moderate diarrhea); and 3, liquid (severe diarrhea) (17). The infectious virus titers were determined by microwell infectivity assay for $TCID_{50}$. Viral RNA in the rectal swab samples was extracted using the MagMax RNA isolation kit (Austin, CA) and MagMAX Express instrument (Termofsher, Waltham, MA) according to the manufacturer's instructions, and viral RNA shedding titers were determined by reverse transcription-quantitative PCR (RT-qPCR) using the OneStep RT-PCR kit (Qiagen, Valencia, CA, USA) with forward and reverse primers (forward, 5′-CGCAAAGACTGAACCCACTAAC-3′; reverse, 5′-TTGCCTCTGTTGTTACTTGGAGAT-3′) and a probe (5′-FAM-TGYYACCAYYACCACGACTCCTGC-BHQ-3′) targeting the N gene (17). The copy number was determined by standard curves.

Immunohistochemical staining. The formalin-fixed duodenum, jejunum and ileum samples were processed as described previously (17). A non-biotin polymerized horseradish peroxidase system (BioGenex Laboratories, San Ramon, CA) was used for IHC staining. Tissues were counterstained with hematoxylin. Monoclonal antibody SD6-29 (gift of Eric Nelson and Steven Lawson, South Dakota State University) targeting PEDV nucleocapsid (N) proteins was used as the primary antibody. For each pig, 10 individual villi of jejunum and ileum were measured, and the ratios of villous height to crypt depth (VH/CD) were calculated (17).

Statistical analysis. The statistical analyses were performed using GraphPad Prism 6.0. Viral genomic RNA and sgmRNAs and the ratio of genomic RNA to $TCID_{50}$ were analyzed by multiple *t* tests. Peak viral shedding, duration of diarrhea, and onset of diarrhea were analyzed by unpaired *t* test. Viral growth kinetics, viral inhibition rate, IFN expression level, and ratio of VH to CD were analyzed by one-way analysis of variance (ANOVA) followed by Tukey's multiple-comparison test.

ACKNOWLEDGMENTS

We thank Juliette Hanson, Ronna Wood, Megan Strother, Sara Tallmadge, Dennis Hartzler, and Jeff Ogg for animal care assistance and Xiaohong Wang for technical assistance. We thank Dongwan Yoo from the University of Illinois at Urbana-Champaign for kindly providing the IPEC-DQ cells.

The project was supported by the National Institute of Food and Agriculture, U.S. Department of Agriculture, under awards 2015-67015-23067 (Q.W., principal investigator [PI]) and 2019-67015-29843 (Q.W., PI).

REFERENCES

1. Wood EN. 1977. An apparently new syndrome of porcine epidemic diarrhoea. Vet Rec 100:243–244. https://doi.org/10.1136/vr.100.12.243.
2. Pensaert MB, De Bouck P. 1978. A new coronavirus-like particle associated with diarrhea in swine. Arch Virol 58:243–247. https://doi.org/10.1007/BF01317606.
3. Li W, Li H, Liu Y, Pan Y, Deng F, Song Y, Tang X, He Q. 2012. New variants of porcine epidemic diarrhea virus, China, 2011. Emerg Infect Dis 18:1350–1353. https://doi.org/10.3201/eid1803.120002.
4. Sun RQ, Cai RJ, Chen YQ, Liang PS, Chen DK, Song CX. 2012. Outbreak of porcine epidemic diarrhea in suckling piglets, China. Emerg Infect Dis 18:161–163. https://doi.org/10.3201/eid1801.111259.
5. Wang D, Fang L, Xiao S. 2016. Porcine epidemic diarrhea in China. Virus Res 226:7–13. https://doi.org/10.1016/j.virusres.2016.05.026.
6. Cima G. 2013. Fighting a deadly pig disease. Industry, veterinarians trying to contain PED virus, new to the US. J Am Vet Med Assoc 243:469–470.

7. Schulz LL, Tonsor GT. 2015. Assessment of the economic impacts of porcine epidemic diarrhea virus in the United States. J Anim Sci 93:5111–5118. https://doi.org/10.2527/jas.2015-9136.
8. Paarlberg PL. 2014. Updated estimated economic welfare impacts of porcine epidemic diarrhea virus (Pedv). Department of Agricultural Economics, Purdue University, West Lafayette, IN.
9. Horzinek MC, Egberink HF, Ederveen J, Callebaut P. 1988. Characterization of the structural proteins of porcine epizootoc diarrhea virus, strain CV777. Am J Vet Res 49:1320–1324.
10. Schoggins JW. 2018. Recent advances in antiviral interferon-stimulated gene biology. F1000Res 7:309. https://doi.org/10.12688/f1000research.12450.1.
11. Zhou JH, Wang YN, Chang QY, Ma P, Hu Y, Cao X. 2018. Type III interferons in viral infection and antiviral immunity. Cell Physiol Biochem 51:173–185. https://doi.org/10.1159/000495172.
12. Kang S, Brown HM, Hwang S. 2018. Direct antiviral mechanisms of interferon-gamma. Immune Netw 18:e33. https://doi.org/10.4110/in.2018.18.e33.
13. Versteeg GA, Bredenbeek PJ, van den Worm SH, Spaan WJ. 2007. Group 2 coronaviruses prevent immediate early interferon induction by protection of viral RNA from host cell recognition. Virology 361:18–26. https://doi.org/10.1016/j.virol.2007.01.020.
14. Zhou H, Perlman S. 2007. Mouse hepatitis virus does not induce beta interferon synthesis and does not inhibit its induction by double-stranded RNA. J Virol 81:568–574. https://doi.org/10.1128/JVI.01512-06.
15. Zhang Q, Shi K, Yoo D. 2016. Suppression of type I interferon production by porcine epidemic diarrhea virus and degradation of CREB-binding protein by nsp1. Virology 489:252–268. https://doi.org/10.1016/j.virol.2015.12.010.
16. Zhang Q, Ke H, Blikslager A, Fujita T, Yoo D. 2018. Type III interferon restriction by porcine epidemic diarrhea virus and the role of viral protein nsp1 in IRF1 signaling. J Virol 92:e01677-17. https://doi.org/10.1128/JVI.01677-17.
17. Hou Y, Ke H, Kim J, Yoo D, Su Y, Boley P, Chepngeno J, Vlasova AN, Saif LJ, Wang Q. 2019. Engineering a live attenuated porcine epidemic diarrhea virus vaccine candidate via inactivation of the viral 2'-O-methyltransferase and the endocytosis signal of the spike protein. J Virol 93:e00406-19. https://doi.org/10.1128/JVI.00406-19.
18. Malone B, Urakova N, Snijder EJ, Campbell EA. 2022. Structures and functions of coronavirus replication-transcription complexes and their relevance for SARS-CoV-2 drug design. Nat Rev Mol Cell Biol 23:21–39. https://doi.org/10.1038/s41580-021-00432-z.
19. Mosca JD, Pitha PM. 1986. Transcriptional and posttranscriptional regulation of exogenous human beta interferon gene in simian cells defective in interferon synthesis. Mol Cell Biol 6:2279–2283. https://doi.org/10.1128/mcb.6.6.2279-2283.1986.
20. Chinese SARS Molecular Epidemiology Consortium. 2004. Molecular evolution of the SARS coronavirus during the course of the SARS epidemic in China. Science 303:1666–1669. https://doi.org/10.1126/science.1092002.
21. Jung K, Saif LJ, Wang Q. 2020. Porcine epidemic diarrhea virus (PEDV): an update on etiology, transmission, pathogenesis, and prevention and control. Virus Res 286:198045. https://doi.org/10.1016/j.virusres.2020.198045.
22. Azhar EI, El-Kafrawy SA, Farraj SA, Hassan AM, Al-Saeed MS, Hashem AM, Madani TA. 2014. Evidence for camel-to-human transmission of MERS coronavirus. N Engl J Med 370:2499–2505. https://doi.org/10.1056/NEJMoa1401505.
23. Hu H, Jung K, Vlasova AN, Chepngeno J, Lu Z, Wang Q, Saif LJ. 2015. Isolation and characterization of porcine deltacoronavirus from pigs with diarrhea in the United States. J Clin Microbiol 53:1537–1548. https://doi.org/10.1128/JCM.00031-15.
24. Pan Y, Tian X, Qin P, Wang B, Zhao P, Yang YL, Wang L, Wang D, Song Y, Zhang X, Huang YW. 2017. Discovery of a novel swine enteric alphacoronavirus (SeACoV) in southern China. Vet Microbiol 211:15–21. https://doi.org/10.1016/j.vetmic.2017.09.020.
25. Crawford K, Lager KM, Kulshreshtha V, Miller LC, Faaberg KS. 2016. Status of vaccines for porcine epidemic diarrhea virus in the United States and Canada. Virus Res 226:108–116. https://doi.org/10.1016/j.virusres.2016.08.005.
26. Langel SN, Paim FC, Lager KM, Vlasova AN, Saif LJ. 2016. Lactogenic immunity and vaccines for porcine epidemic diarrhea virus (PEDV): historical and current concepts. Virus Res 226:93–107. https://doi.org/10.1016/j.virusres.2016.05.016.
27. Song DS, Oh JS, Kang BK, Yang JS, Moon HJ, Yoo HS, Jang YS, Park B. 2007. Oral efficacy of Vero cell attenuated porcine epidemic diarrhea virus DR13 strain. Res Vet Sci 82:134–140. https://doi.org/10.1016/j.rvsc.2006.03.007.
28. Lei X, Dong X, Ma R, Wang W, Xiao X, Tian Z, Wang C, Wang Y, Li L, Ren L, Guo F, Zhao Z, Zhou Z, Xiang Z, Wang J. 2020. Activation and evasion of type I interferon responses by SARS-CoV-2. Nat Commun 11:3810. https://doi.org/10.1038/s41467-020-17665-9.
29. Narayanan K, Ramirez SI, Lokugamage KG, Makino S. 2015. Coronavirus nonstructural protein 1: common and distinct functions in the regulation of host and viral gene expression. Virus Res 202:89–100. https://doi.org/10.1016/j.virusres.2014.11.019.
30. Snijder EJ, Bredenbeek PJ, Dobbe JC, Thiel V, Ziebuhr J, Poon LL, Guan Y, Rozanov M, Spaan WJ, Gorbalenya AE. 2003. Unique and conserved features of genome and proteome of SARS-coronavirus, an early split-off from the coronavirus group 2 lineage. J Mol Biol 331:991–1004. https://doi.org/10.1016/S0022-2836(03)00865-9.
31. Almeida MS, Johnson MA, Wüthrich K. 2006. NMR assignment of the SARS-CoV protein nsp1. J Biomol NMR 36:46–46. https://doi.org/10.1007/s10858-006-9018-9.
32. Jansson AM. 2013. Structure of alphacoronavirus transmissible gastroenteritis virus nsp1 has implications for coronavirus nsp1 function and evolution. J Virol 87:2949–2955. https://doi.org/10.1128/JVI.03163-12.
33. Shen Z, Ye G, Deng F, Wang G, Cui M, Fang L, Xiao S, Fu ZF, Peng G. 2018. Structural basis for the inhibition of host gene expression by porcine epidemic diarrhea virus nsp1. J Virol 92:e01896-17. https://doi.org/10.1128/JVI.01896-17.
34. Kamitani W, Huang C, Narayanan K, Lokugamage KG, Makino S. 2009. A two-pronged strategy to suppress host protein synthesis by SARS coronavirus Nsp1 protein. Nat Struct Mol Biol 16:1134–1140. https://doi.org/10.1038/nsmb.1680.
35. Kamitani W, Narayanan K, Huang C, Lokugamage K, Ikegami T, Ito N, Kubo H, Makino S. 2006. Severe acute respiratory syndrome coronavirus nsp1 protein suppresses host gene expression by promoting host mRNA degradation. Proc Natl Acad Sci U S A 103:12885–12890. https://doi.org/10.1073/pnas.0603144103.
36. Narayanan K, Huang C, Lokugamage K, Kamitani W, Ikegami T, Tseng CTK, Makino S. 2008. Severe acute respiratory syndrome coronavirus nsp1 suppresses host gene expression, including that of type I interferon, in infected cells. J Virol 82:4471–4479. https://doi.org/10.1128/JVI.02472-07.
37. Wathelet MG, Orr M, Frieman MB, Baric RS. 2007. Severe acute respiratory syndrome coronavirus evades antiviral signaling: role of nsp1 and rational design of an attenuated strain. J Virol 81:11620–11633. https://doi.org/10.1128/JVI.00702-07.
38. Nakagawa K, Narayanan K, Wada M, Popov VL, Cajimat M, Baric RS, Makino S. 2018. The endonucleolytic RNA cleavage function of nsp1 of Middle East respiratory syndrome coronavirus promotes the production of infectious virus particles in specific human cell lines. J Virol 92:e01157-18. https://doi.org/10.1128/JVI.01157-18.
39. Clark LK, Green TJ, Petit CM. 2021. Structure of nonstructural protein 1 from SARS-CoV-2. J Virol 95:e02019-20. https://doi.org/10.1128/JVI.02019-20.
40. Zhang K, Miorin L, Makio T, Dehghan I, Gao S, Xie Y, Zhong H, Esparza M, Kehrer T, Kumar A, Hobman TC, Ptak C, Gao B, Minna JD, Chen Z, García-Sastre A, Ren Y, Wozniak RW, Fontoura BMA. 2021. Nsp1 protein of SARS-CoV-2 disrupts the mRNA export machinery to inhibit host gene expression. Sci Adv 7:eabe7386. https://doi.org/10.1126/sciadv.abe7386.
41. Schubert K, Karousis ED, Jomaa A, Scaiola A, Echeverria B, Gurzeler LA, Leibundgut M, Thiel V, Mühlemann O, Ban N. 2020. SARS-CoV-2 Nsp1 binds the ribosomal mRNA channel to inhibit translation. Nat Struct Mol Biol 27:959–966. https://doi.org/10.1038/s41594-020-0511-8.
42. Thoms M, Buschauer R, Ameismeier M, Koepke L, Denk T, Hirschenberger M, Kratzat H, Hayn M, Mackens-Kiani T, Cheng J, Straub JH, Stürzel CM, Fröhlich T, Berninghausen O, Becker T, Kirchhoff F, Sparrer KMJ, Beckmann R. 2020. Structural basis for translational shutdown and immune evasion by the Nsp1 protein of SARS-CoV-2. Science 369:1249–1255. https://doi.org/10.1126/science.abc8665.
43. Shen Z, Wang G, Yang Y, Shi J, Fang L, Li F, Xiao S, Fu ZF, Peng G. 2019. A conserved region of nonstructural protein 1 from alphacoronaviruses inhibits host gene expression and is critical for viral virulence. J Biol Chem 294:13606–13618. https://doi.org/10.1074/jbc.RA119.009713.
44. Deng X, Buckley AC, Pillatzki A, Lager KM, Faaberg KS, Baker SC. 2020. Inactivating three interferon antagonists attenuates pathogenesis of an enteric coronavirus. J Virol 94:e00565-20. https://doi.org/10.1128/JVI.00565-20.
45. Hou Y, Meulia T, Gao X, Saif LJ, Wang Q. 2019. Deletion of both the tyrosine-based endocytosis signal and the endoplasmic reticulum retrieval signal in the cytoplasmic tail of spike protein attenuates porcine epidemic diarrhea virus in pigs. J Virol 93:e01758-18. https://doi.org/10.1128/JVI.01758-18.
46. Pene F, Merlat A, Vabret A, Rozenberg F, Buzyn A, Dreyfus F, Cariou A, Freymuth F, Lebon P. 2003. Coronavirus 229E-related pneumonia in immunocompromised patients. Clin Infect Dis 37:929–932. https://doi.org/10.1086/377612.

47. Chiu SS, Hung Chan K, Wing Chu K, Kwan SW, Guan Y, Man Poon LL, Peiris JSM. 2005. Human coronavirus NL63 infection and other coronavirus infections in children hospitalized with acute respiratory disease in Hong Kong, China. Clin Infect Dis 40:1721–1729. https://doi.org/10.1086/430301.
48. Dijkman R, Jebbink MF, Koekkoek SM, Deijs M, Jónsdóttir HR, Molenkamp R, Ieven M, Goossens H, Thiel V, van der Hoek L. 2013. Isolation and characterization of current human coronavirus strains in primary human epithelial cell cultures reveal differences in target cell tropism. J Virol 87:6081–6090. https://doi.org/10.1128/JVI.03368-12.
49. Woo PCY, Lau SKP, Tsoi H-W, Huang Y, Poon RWS, Chu C-M, Lee RA, Luk W-K, Wong GKM, Wong BHL, Cheng VCC, Tang BSF, Wu AKL, Yung RWH, Chen H, Guan Y, Chan K-H, Yuen K-Y. 2005. Clinical and molecular epidemiological features of coronavirus HKU1-associated community-acquired pneumonia. J Infect Dis 192:1898–1907. https://doi.org/10.1086/497151.
50. Al-Tawfiq JA, Hinedi K, Ghandour J, Khairalla H, Musleh S, Ujayli A, Memish ZA. 2014. Middle East respiratory syndrome coronavirus: a case-control study of hospitalized patients. Clin Infect Dis 59:160–165. https://doi.org/10.1093/cid/ciu226.
51. Peiris JSM, Lai ST, Poon LLM, Guan Y, Yam LYC, Lim W, Nicholls J, Yee WKS, Yan WW, Cheung MT, Cheng VCC, Chan KH, Tsang DNC, Yung RWH, Ng TK, Yuen KY. 2003. Coronavirus as a possible cause of severe acute respiratory syndrome. Lancet 361:1319–1325. https://doi.org/10.1016/S0140-6736(03)13077-2.
52. Andersen KG, Rambaut A, Lipkin WI, Holmes EC, Garry RF. 2020. The proximal origin of SARS-CoV-2. Nat Med 26:450–452. https://doi.org/10.1038/s41591-020-0820-9.
53. Lam TT-Y, Jia N, Zhang Y-W, Shum MH-H, Jiang J-F, Zhu H-C, Tong Y-G, Shi Y-X, Ni X-B, Liao Y-S, Li W-J, Jiang B-G, Wei W, Yuan T-T, Zheng K, Cui X-M, Li J, Pei G-Q, Qiang X, Cheung WY-M, Li L-F, Sun F-F, Qin S, Huang J-C, Leung GM, Holmes EC, Hu Y-L, Guan Y, Cao W-C. 2020. Identifying SARS-CoV-2-related coronaviruses in Malayan pangolins. Nature 583:282–285. https://doi.org/10.1038/s41586-020-2169-0.
54. Vlasova AN, Diaz A, Damtie D, Xiu L, Toh TH, Lee JSY, Saif LJ, Gray GC. 2022. Novel canine coronavirus isolated from a hospitalized pneumonia patient, East Malaysia. Clin Infect Dis 74:446–454. https://doi.org/10.1093/cid/ciab456.
55. Lednicky JA, Tagliamonte MS, White SK, Blohm GM, Alam MM, Iovine NM, Salemi M, Mavian C, Morris JG. 2021. Isolation of a novel recombinant canine coronavirus from a visitor to Haiti: further evidence of transmission of coronaviruses of zoonotic origin to humans. Clin Infect Dis. https://doi.org/10.1093/cid/ciab924.
56. Lednicky JA, Tagliamonte MS, White SK, Elbadry MA, Alam MM, Stephenson CJ, Bonny TS, Loeb JC, Telisma T, Chavannes S, Ostrov DA, Mavian C, Beau De Rochars VM, Salemi M, Morris JG. 2021. Independent infections of porcine deltacoronavirus among Haitian children. Nature 600:133–137. https://doi.org/10.1038/s41586-021-04111-z.
57. Edwards CE, Yount BL, Graham RL, Leist SR, Hou YJ, Dinnon KH, Sims AC, Swanstrom J, Gully K, Scobey TD, Cooley MR, Currie CG, Randell SH, Baric RS. 2020. Swine acute diarrhea syndrome coronavirus replication in primary human cells reveals potential susceptibility to infection. Proc Natl Acad Sci U S A 117:26915–26925. https://doi.org/10.1073/pnas.2001046117.
58. George S, Deshpande GR, Sapkal GN. 2020. Interferons and their role in viral infection. *In* Bramhachari PV (ed), Dynamics of immune activation in viral diseases, p 61–80. Springer, Singapore.
59. Saif LJ. 1999. Enteric viral infections of pigs and strategies for induction of mucosal immunity. Adv Vet Med 41:429–446. https://doi.org/10.1016/S0065-3519(99)80033-0.
60. Niu X, Hou YJ, Jung K, Kong F, Saif LJ, Wang Q. 2021. Chimeric porcine deltacoronaviruses with sparrow coronavirus spike protein or the receptor-binding domain infect pigs but lose virulence and intestinal tropism. Viruses 13:122. https://doi.org/10.3390/v13010122.
61. Annamalai T, Lin CM, Gao X, Liu X, Lu Z, Saif LJ, Wang Q. 2017. Cross protective immune responses in nursing piglets infected with a US spike-insertion deletion porcine epidemic diarrhea virus strain and challenged with an original US PEDV strain. Vet Res 48:61–68. https://doi.org/10.1186/s13567-017-0469-7.
62. Reed LJ, Muench H. 1938. A simple method of estimating fifty per cent endpoints. American J Epidemiology 27:493–497. https://doi.org/10.1093/oxfordjournals.aje.a118408.
63. Livak KJ, Schmittgen TD. 2001. Analysis of relative gene expression data using real-time quantitative PCR and the $2-\Delta\Delta CT$ method. Methods 25:402–408. https://doi.org/10.1006/meth.2001.1262.
64. Liu X, Lin CM, Annamalai T, Gao X, Lu Z, Esseili MA, Jung K, El-Tholoth M, Saif LJ, Wang Q. 2015. Determination of the infectious titer and virulence of an original US porcine epidemic diarrhea virus PC22A strain. Vet Res 46:109. https://doi.org/10.1186/s13567-015-0249-1.
65. Hou Y, Lin CM, Yokoyama M, Yount BL, Marthaler D, Douglas AL, Ghimire S, Qin Y, Baric RS, Saif LJ, Wang Q. 2017. Deletion of a 197-amino-acid region in the N-terminal domain of spike protein attenuates porcine epidemic diarrhea virus in piglets. J Virol 91:e00227-17. https://doi.org/10.1128/JVI.00227-17.